Eccentrically loaded single angle columns

Autor(en): **Usami, Tsutomu / Galambos, Theodore V.**

Objekttyp: **Article**

Zeitschrift: **IABSE publications = Mémoires AIPC = IVBH Abhandlungen**

Band (Jahr): **31 (1971)**

PDF erstellt am: **26.09.2024**

Persistenter Link: https://doi.org/10.5169/seals-24223

Nutzungsbedingungen

Die ETH-Bibliothek ist Anbieterin der digitalisierten Zeitschriften. Sie besitzt keine Urheberrechte an den Inhalten der Zeitschriften. Die Rechte liegen in der Regel bei den Herausgebern.
Die auf der Plattform e-periodica veröffentlichten Dokumente stehen für nicht-kommerzielle Zwecke in Lehre und Forschung sowie für die private Nutzung frei zur Verfügung. Einzelne Dateien oder Ausdrucke aus diesem Angebot können zusammen mit diesen Nutzungsbedingungen und den korrekten Herkunftsbezeichnungen weitergegeben werden.
Das Veröffentlichen von Bildern in Print- und Online-Publikationen ist nur mit vorheriger Genehmigung der Rechteinhaber erlaubt. Die systematische Speicherung von Teilen des elektronischen Angebots auf anderen Servern bedarf ebenfalls des schriftlichen Einverständnisses der Rechteinhaber.

Haftungsausschluss

Alle Angaben erfolgen ohne Gewähr für Vollständigkeit oder Richtigkeit. Es wird keine Haftung übernommen für Schäden durch die Verwendung von Informationen aus diesem Online-Angebot oder durch das Fehlen von Informationen. Dies gilt auch für Inhalte Dritter, die über dieses Angebot zugänglich sind.

Ein Dienst der *ETH-Bibliothek*
ETH Zürich, Rämistrasse 101, 8092 Zürich, Schweiz, www.library.ethz.ch

http://www.e-periodica.ch

Eccentrically Loaded Single Angle Columns

Colonnes composées de cornières chargées excentriquement

Aussermittig belastete Stahlstützen aus einzelnen Winkelprofilen

TSUTOMU USAMI
Lecturer of Civil Engrg., University of Gifu, Gifu, Japan; formerly Research Assistant, Washington Univ., St. Louis, Mo., U.S.A.

THEODORE V. GALAMBOS
M. ASCE, Prof. of Civil Engrg., Washington Univ., St. Louis, Mo., U.S.A.

Introduction

A design method for single angle compression members used as web members in long span steel joists has been reported in reference [6][1]) based on a series of column tests of steel angles. This paper is to provide the theoretical basis to the test results. The single angle compression members are treated as end-restrained columns with biaxially eccentric load, and a method of numerical analysis for determining the elastic-plastic behavior of such columns is presented. The analysis allows for the effects of residual stresses and initial deflections of columns. A comprehensive review has been reported by CHEN and SANTATHADOPORN [2] on literatures dealing with inelastic behavior of biaxially loaded columns, but it seems that no work has previously been made on the subject reported in this paper. Recently TRAHAIR [9] published a general method of elastic analysis of restrained columns loaded eccentrically with respect to both principal axes of the end cross sections, and compared its solutions with the test results of single angle columns [8]. Trahair's method of analysis is extended in this paper to allow for the inelastic effects of columns.

Shown in Fig. 1 is a typical joint of a long span steel joist where single angle members are used as its web members. The restraining member represents a gusset plate or a web plate of chord member (structural Tee, for example). Such a single angle compression member is idealized as shown in

---

[1]) Numericals in parentheses refer to corresponding items in the Appendix IV; References.

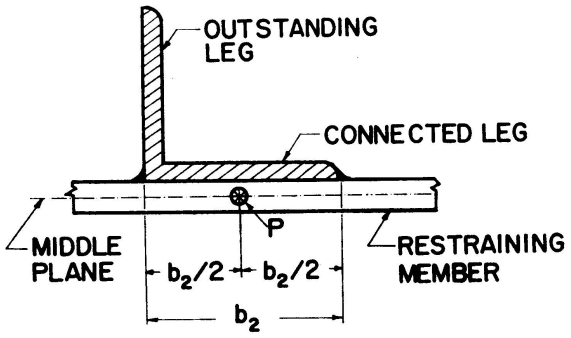

Fig. 1. Joint of a Truss.

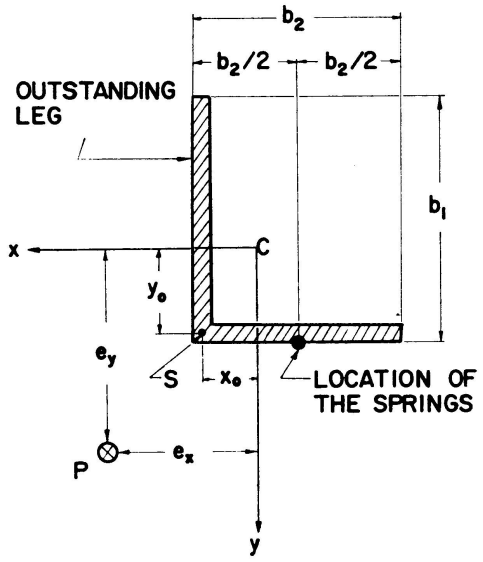

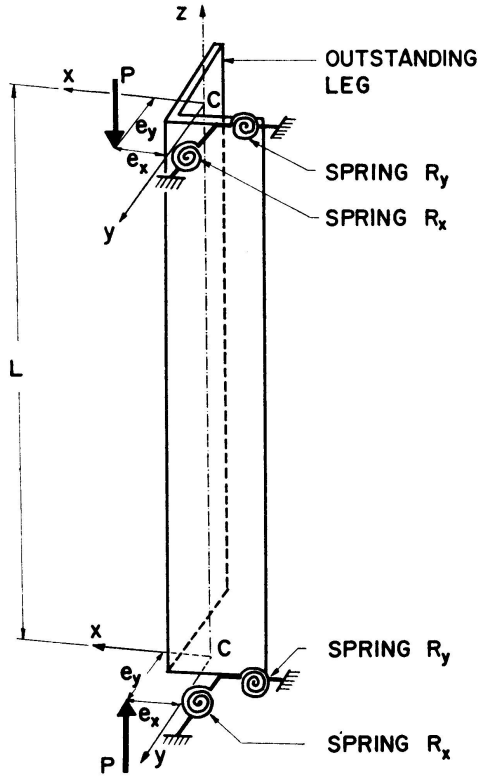

Fig. 2. Idealized Single Angle Column.

Fig. 3. End Cross Section of Angle Column.

Figs. 2 and 3 for the purpose of subsequent analysis. The column is loaded by an axial thrust P with eccentricities e_x and e_y. The axes x and y are centroidal axes of the angle (its centroid is denoted by C), and are, respectively, parallel to the connected leg and the outstanding leg of the angle. The axis z is the centroidal longitudinal axis of the column. The end restraints, which are provided by the rotational stiffnesses of the restraining member in its plane and out of its plane, are, respectively, replaced by the equivalent rotational springs of stiffnesses R_y and R_x.

Assumptions and Conditions

The following assumptions are made in the subsequent analysis:

1. A second order analysis is performed, i.e., equilibrium is formulated on the deformed column.
2. The column is prismatic and of a thin-walled angle cross-section (Fig. 2).
3. The stress-strain diagram of the member is elastic-perfectly plastic (Fig. 4).

4. Yielding is initiated by normal stress only.
5. The axial thrust P, acting at the column ends with the eccentricities e_x and e_y as shown in Figs. 2 and 3, retains its original direction throughout the loading history.

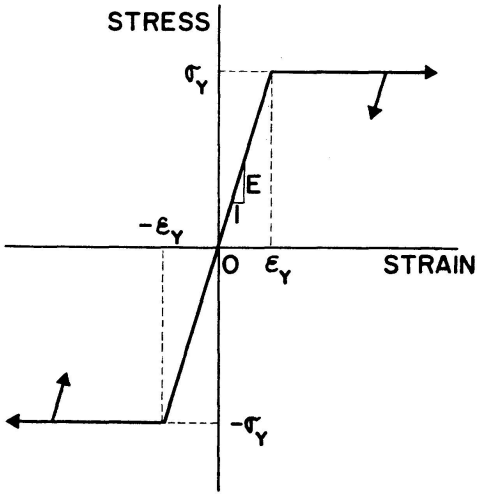

Fig. 4. Assumed Stress-Strain Diagram of the Column Material.

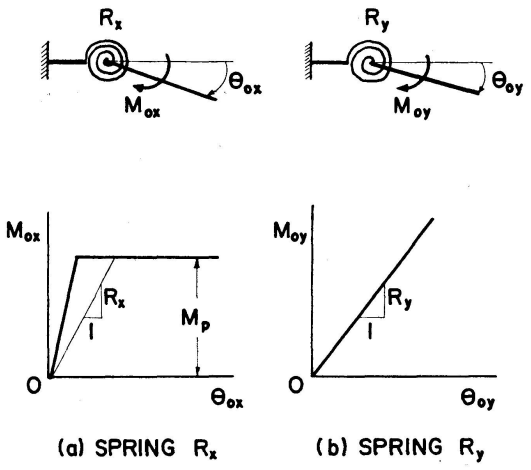

Fig. 5. Characteristics of the Rotational Springs.

6. The column ends are prevented both from translating horizontally and from twisting, and the end rotations are restrained by the rotational springs in such positions and directions as shown in Figs. 2 and 3.
7. The end moment versus end rotation characteristics of the rotational springs about the x and y axes are, respectively, assumed to be as shown in Figs. 5a and 5b. The end moments M_{0x} and M_{0y} about the x and y axes are, respectively, related to the corresponding end rotations θ_{0x} and θ_{0y} about these axes by

$$M_{0x} = R_x \theta_{0x}, \tag{1a}$$

$$M_{0y} = R_y \theta_{0y}, \tag{1b}$$

in which the stiffnesses R_x and R_y are, respectively, given by the secant moduli of the $M_{0x}-\theta_{0x}$ and $M_{0y}-\theta_{0y}$ relations.

8. The warping strains due to non-uniform torsion are ignored [5].
9. The center of twist of the cross-section of the column is coincident with the shear center regardless of the elastic and inelastic range of the column.
10. St. Venant torsional rigidity retains its original elastic value in the inelastic range. The validity of assumption 10 is discussed in reference [10].

The following specific conditions are furthermore allowed for in the analysis:

1. Cooling residual stresses.
2. Initial displacements symmetrical with respect to the column center.
3. Axial stresses locked in the column due to initial displacements of the column.

The cooling residual stress, σ_R are assumed to be uniform along the whole length of the column for each fiber and must satisfy the following conditions:

$$\int_A \sigma_R dA = \int_A \sigma_R y dA = \int_A \sigma_R x dA = 0. \tag{2}$$

Initial displacements are assumed to exist in the x and y directions, being, respectively, denoted by u_I and v_I, and they are assumed to be zero at the column ends. No initial twist is considered. Axial stresses σ_I due to the initial displacements are induced in the column when the end slopes of the initial displacements are not zero as well as when the column ends are not allowed to rotate freely due to the end restraints. Since no restraint to vertical movement is assumed, σ_I will not produce a longitudinal resultant force and thus

$$\int_A \sigma_I dA = 0. \tag{3a}$$

The stresses σ_I, however, produce bending moments abcut the x and y axes which are expressed by

$$M_{Ix} = \int_A \sigma_I y dA, \tag{3b}$$

$$M_{Iy} = -\int_A \sigma_I x dA. \tag{3c}$$

These bending moments are stored in the rotational springs as initial restraining moments, and are also locked in the column itself. Finally it is assumed that the algebraic sum of σ_R and σ_I does not exceed the yield stress of the material anywhere in the column.

Mathematical Formulation

Internal Axial Force and Moments

Let Fig. 6 show an angle member of unit length loaded by axial force P^* acting at the centroid and by three components of moments, M_x^*, M_y^* and M_z^*. These forces will produce axial strains and shear strains in the member. Because the warping strains due to non-uniform torsion are ignored and because the contribution of torsional shear stresses to yielding is also neglected, the response of the element to the moment M_z^* may be treated separately. Accordingly, an axial strain ϵ^* of a point in the member may be written as

$$\epsilon^* = -\epsilon_c^* - \Phi_x^* x + \Phi_y^* y + \frac{\sigma_R}{E} + \frac{\sigma_I}{E}, \tag{4}$$

in which ϵ_c^* denotes the axial compressive strain at the centroid, Φ_x^* curvature in the x-z plane, Φ_y^* curvature in the y-z plane and E the modulus of elasticity. When the applied force and moments change a small amount the axial strain

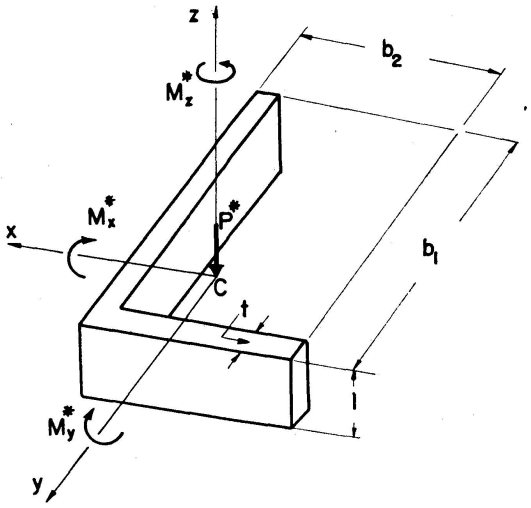

Fig. 6. Angle Member Subjected to Axial Force and Moments.

will also undergo a certain change which is expressed by

$$\delta\epsilon = -\delta\epsilon_c - \delta\Phi_x x + \delta\Phi_y y, \tag{5}$$

where $\delta\epsilon$, $\delta\epsilon_c$, $\delta\Phi_x$ and $\delta\Phi_y$ denote increments of ϵ^*, ϵ_c^*, Φ_x^* and Φ_y^*, respectively. The axial strain ϵ^* and its increment $\delta\epsilon$ may be resolved into the elastic strain component, which is related to the corresponding stress by Hook's law, and the plastic strain component:

$$\epsilon^* = \frac{\sigma^*}{E} + \epsilon^{*p}, \tag{6a}$$

$$\delta\epsilon = \frac{\delta\epsilon}{E} + \delta\epsilon^p, \tag{6b}$$

in which the quantities with superscript p indicate the plastic strain components, and σ^* and $\delta\sigma$ denote the axial stresses corresponding to ϵ^* and $\delta\epsilon$, respectively. The plastic strain component $\delta\epsilon^p$ is expressed by

$$\begin{aligned}
&\delta\epsilon^p = 0, \quad \text{when } |\epsilon^* + \delta\epsilon| \leqq \epsilon_Y, \\
&\delta\epsilon^p = (\epsilon^* + \delta\epsilon) - \epsilon_Y \operatorname{sgn}(\epsilon^* + \delta\epsilon), \quad \text{when } |\epsilon^*| \leqq \epsilon_Y \text{ and } |\epsilon^* + \delta\epsilon| \geqq \epsilon_Y, \\
&\delta\epsilon^p = \delta\epsilon, \quad \text{when } |\epsilon^*| \geqq \epsilon_Y \text{ and } |\epsilon^* + \delta\epsilon| \geqq \epsilon_Y, \\
&\delta\epsilon^p = 0, \quad \text{when } |\epsilon^*| \geqq |\epsilon^* + \delta\epsilon|,
\end{aligned} \tag{7}$$

in which ϵ_Y denotes the yield strain of the material and sgn denotes the signum function (i.e., $\operatorname{sgn} x = 1$ for $x > 0$, $\operatorname{sgn} x = -1$ for $x < 0$ and $\operatorname{sgn} x = 0$ for $x = 0$). The plastic strain component ϵ^{*p} is expressed by a sum of the plastic strains $\delta\epsilon^p$ up to the loading stage P^*, M_x^* and M_y^*, that is

$$\epsilon^{*p} = \sum \delta\epsilon^p, \tag{8}$$

in which $\sum$ denotes a summation of $\delta\epsilon^p$ till the applied force and moments reach P^*, M_x^* and M_y^*. From Eqs. (4), (5) and (6), the total axial stress σ of a point in the member after the change of the applied force and moments is obtained as

$$\sigma = \sigma^* + \delta\sigma = E(-\epsilon_c - \Phi_x + \Phi_y y) + \sigma_R + \sigma_I - E(\epsilon^{*p} + \delta\epsilon^p), \tag{9}$$

where $\epsilon_c = \epsilon_c^* + \delta\epsilon_c, \Phi_x = \Phi_x^* + \delta\Phi_x$ and $\Phi_y = \Phi_y^* + \delta\Phi_y$, and they represent the corresponding quantities after the change of the applied force and moments. The axial stress σ produces the following cross-sectional forces:

$$P = -\int_A \sigma\, dA, \qquad M_x = \int_A \sigma y\, dA, \qquad M_y = -\int_A \sigma x\, dA.$$

Substituting Eq. (9) into the above equations, and considering Eqs. (2) and (3) and the fact that the x and y axes are centroidal axes, these forces become equal to:

$$P = E[A\epsilon_c + \Gamma], \tag{10a}$$

$$M_x = E[-I_{xy}\Phi_x + I_x\Phi_y - \Gamma_x] + M_{Ix}, \tag{10b}$$

$$M_y = E[I_y\Phi_x - I_{xy}\Phi_y + \Gamma_y] - M_{IY}, \tag{10c}$$

in which

$$\begin{aligned}
I_x &= \int_A y^2\, dA, & I_y &= \int_A x^2\, dA, & I_{xy} &= \int_A xy\, dA,\\
\Gamma &= \Gamma^* + \delta\Gamma, & \Gamma^* &= \int_A \epsilon^{*p}\, dA, & \delta\Gamma &= \int_A \delta\epsilon^p\, dA,\\
\Gamma_y &= \Gamma_y^* + \delta\Gamma_y, & \Gamma_y^* &= \int_A \epsilon^{*p} x\, dA, & \delta\Gamma_y &= \int_A \delta\epsilon^p x\, dA,\\
\Gamma_x &= \Gamma_x^* + \delta\Gamma_x, & \Gamma_x^* &= \int_A \epsilon^{*p} y\, dA, & \delta\Gamma_x &= \int_A \delta\epsilon^p y\, dA.
\end{aligned} \tag{11}$$

Owing to assumptions 4, 8 and 10, the moment M_z is independent of the axial stress σ and is given by

$$M_z = GK_T\phi', \tag{10d}$$

where the prime indicates differentiation with respect to the z-coordinate. This is the same expression as the elastic St. Venant's torsion.

External Axial Force and Moments

Fig. 7 shows the coordinate systems used in the following derivations. The x-y-z coordinate system is the same as defined in Fig. 2, and is fixed in space. The centroidal axes of the initially displaced cross-sections are denoted by the x' and y' axes. The x' and y' axes are, respectively, parallel to the connected leg and the outstanding leg of the angle column. The initial deflections u_I and v_I are measured as shown in the figures. The ξ, η and ζ axes are used to denote the displaced x', y' and z axes. The ξ and η axes are centroidal axes and are parallel to the connected leg and the outstanding leg of the angle, respectively. The ζ axis is tangent to the displaced centroidal longitudinal axis of the column. The displacements and angle of twist of the shear center S due to loading are denoted by u, v and ϕ; u and v are the displacements in the x' and y' direc-

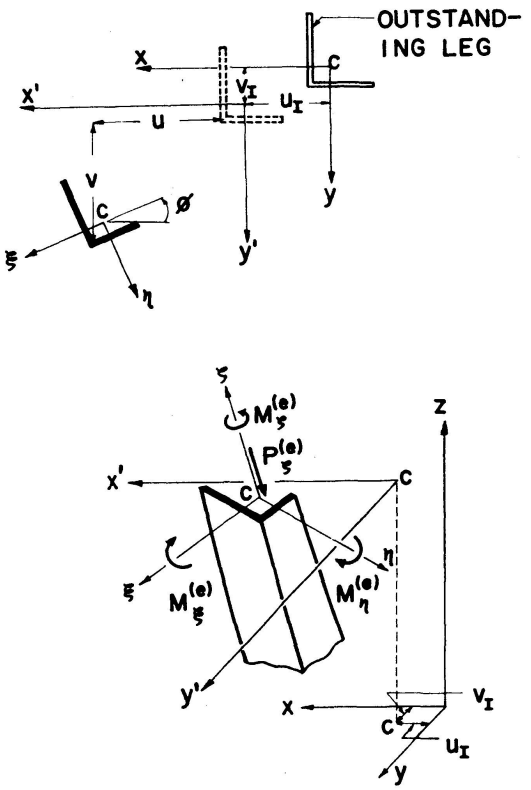

Fig. 7. Coordinate Systems and Sign Convention for External Force and Moments.

tions, and ϕ is the angle of twist about the z-axis. Because of the symmetrical nature of the column dimensions and of loading, the deformed configuration of the column is symmetrical with respect to the column center. The end restraining moments, which are induced by virtue of the rotational springs, are also alike at both ends. Each of the restraining moments is made up of two components: one is due to loading and the other is due to the fact that the end slopes of the initially deformed column are not usually zero. These latter restraining moments are already defined as M_{Ix} and M_{Iy} in Eqs. (3a) and (3b), respectively. The restraining moments about the x and y axes due to load are denoted by $\overline{M}_{0x}$ and $\overline{M}_{0y}$, respectively, which are expressed in terms of the corresponding stiffness of spring and end slope at the location of the rotational springs (see Fig. 3) as follows:

$$\overline{M}_{0x} = -R_x\left(v_0' - \frac{b_2}{2}\phi_0'\right), \tag{12a}$$

$$\overline{M}_{0y} = R_y u_0', \tag{12b}$$

where the subscript 0 refers to the column end and b_2 denotes the length of the connected leg. Similar relations are obtained for the initial restraining moments M_{Ix} and M_{Iy} as follows:

$$M_{Ix} = -R_x v_{I0}' \tag{13a}$$

$$M_{Iy} = R_y u_{I0}' \tag{13b}$$

Equivalent eccentricities are defined by the following equations:

$$\bar{e}_y = e_y - \frac{M_{Ix}}{P} - \frac{\bar{M}_{0x}}{P} = e_y + \frac{R_x}{P}\left(v_0' + v_{I0}' - \frac{b_2}{2}\phi_0'\right), \tag{14a}$$

$$\bar{e}_x = e_x + \frac{M_{Iy}}{P} + \frac{\bar{M}_{0y}}{P} = e_x + \frac{R_y}{P}\,u_0' + u_{I0}'), \tag{14b}$$

where $\bar{e}_x$ and $\bar{e}_y$ are the equivalent eccentricities corresponding to e_x and e_y, respectively. By using the equivalent eccentricities in place of the real eccentricities of the axial thrust P, the column may be analyzed as if both ends were flexurally pinned and as if the axial thrust P were applied to the column with the eccentricities $\bar{e}_x$ and $\bar{e}_y$. The expressions for the external axial force and moments of the "replaced" column in the presence of initial displacements have been derived by CULVER [3], and they are equal to:

$$P_\zeta^{(e)} = P, \tag{15a}$$

$$M_\xi^{(e)} = P\{(v+v_I) - \bar{e}_y - (x_0 - \bar{e}_x)\,\phi\}, \tag{15b}$$

$$M_\eta^{(e)} = -P\{(u+u_I) - \bar{e}_x + (y_0 - \bar{e}_y)\,\phi\}, \tag{15c}$$

$$M_\zeta^{(e)} = P\,(y_0 - \bar{e}_y)\,(u' + u_I') - P\,(x_0 - \bar{e}_x)\,(v' + v_I') - \bar{K}\,\phi', \tag{15d}$$

where $P_\zeta^{(e)}$, $M_\xi^{(e)}$, $M_\eta^{(e)}$ and $M_\zeta^{(e)}$ represent external axial force and external moments about the ξ, η and ζ axes, respectively, and x_0 and y_0 are coordinates of the shear center in the x-y coordinate system. The quantity $\bar{K}$ is defined by

$$\bar{K} = \int_A \sigma\{(x-x_0)^2 + (y-y_0)^2\}\,dA, \tag{16}$$

where σ is given in Fig. 9. Substituting the expressions for σ into Eq. (16) and using Eqs. (10b) and (10c) with the approximation

$$M_x \cong -P\bar{e}_y \quad \text{and} \quad M_y \cong P\bar{e}_x$$

the following expression for $\bar{K}$ is obtained:

$$\bar{K} = -(P r_s^2 + E\Lambda) + \bar{K}_R + \bar{K}_I, \tag{17}$$

where

$$\begin{aligned} r_s^2 &= r_0^2 + \left\{\left(\bar{e}_x - \frac{M_{Iy}}{P}\right) - \frac{I_{xy}}{I_x}\left(\bar{e}_y + \frac{M_{Ix}}{P}\right)\right\}\beta_y \\ &\quad + \left\{\left(\bar{e}_y + \frac{M_{Ix}}{P}\right) - \frac{I_{xy}}{I_y}\left(\bar{e}_x - \frac{M_{Iy}}{P}\right)\right\}\beta_x, \end{aligned} \tag{18a}$$

$$r_0^2 = x_0^2 + y_0^2 + \frac{I_x + I_y}{A}, \tag{18b}$$

$$\beta_x = \frac{1}{1 - I_{xy}^2/I_x I_y}\left\{\frac{\int_A y\,(x^2+y^2)\,dA}{I_x} - 2y_0 - 2x_0\frac{I_{xy}}{I_x}\right\}, \tag{18c}$$

$$\beta_y = \frac{1}{1 - I_{xy}^2/I_x I_y}\left\{\frac{\int_A x\,(x^2+y^2)\,dA}{I_y} - 2x_0 - 2y_0\frac{I_{xy}}{I_y}\right\}, \tag{18d}$$

$$\bar{K}_R = \int_A \sigma_R (x^2+y^2)\, dA\,, \tag{18e}$$

$$\bar{K}_I = \int_A \sigma_I \{(x-x_0)^2+(y-y_0)^2\}\, dA\,, \tag{18f}$$

$$\Lambda = \Lambda^* + \delta\Lambda\,, \tag{18g}$$

$$\begin{aligned}\Lambda^* = &-\frac{I_x+I_y}{A}\Gamma^* - \left(\beta_x - \beta_y \frac{I_{xy}}{I_x} + 2x_0\right)\Gamma_x^* \\ &- \left(\beta_y - \beta_x \frac{I_{xy}}{I_y} + 2y_0\right)\Gamma_y^* + \int_A \epsilon^{*p}(x^2+y^2)\, dA\,,\end{aligned} \tag{18h}$$

$$\begin{aligned}\delta\Lambda = &-\frac{I_x+I_y}{A}\delta\Gamma - \left(\beta_x - \beta_y \frac{I_{xy}}{I_x} + 2x_0\right)\delta\Gamma_x \\ &- \left(\beta_y - \beta_x \frac{I_{xy}}{I_y} + 2y_0\right)\delta\Gamma_y + \int_A \delta\epsilon^p (x^2+y^2)\, dA\,.\end{aligned} \tag{18i}$$

Equilibrium Equations

Since small deformations are assumed, the curvatures in the ξ-ζ plane, Φ_ξ, and in the η-ζ plane, Φ_η, are expressed by

$$\Phi_\xi \cong \Phi_x \cong u''\,, \tag{19a}$$

$$\Phi_\eta \cong \Phi_y \cong -v''\,. \tag{19b}$$

Equating Eqs. (10a)–(10c) to Eqs. (15a)–(15c), respectively and using Eqs. (17) and (19) yield the following equilibrium equations:

$$P = EA\left(\epsilon_c + \frac{\Gamma}{A}\right), \tag{20a}$$

$$EI_x v'' + EI_{xy} u'' + P v - P(x_0 - \bar{e}_x)\phi = P\bar{e}_y - P v_I + M_{Ix} - E\Gamma_x, \tag{20b}$$

$$EI_y u'' + EI_{xy} v'' + P u + P(y_0 - \bar{e}_y)\phi = P\bar{e}_x - P u_I - M_{Iy} - E\Gamma_y. \tag{20c}$$

The fourth equilibrium equation may be obtained by equating Eq. (10d) to Eq. (15d) and by differentiating both sides once with respect to z, that is.

$$\begin{aligned}P(x_0-\bar{e}_x)v'' - P(y_0-\bar{e}_y)u'' + (GK_T + \bar{K}_R + \bar{K}_I - Pr_s^2)\phi'' = \\ E\Lambda\phi'' - P(x_0-\bar{e}_x)v_I'' + P(y_0-\bar{e}_y)u_I''\,.\end{aligned} \tag{20d}$$

In deriving Eq. (20d), an approximation

$$\frac{d}{dz}(E\Lambda\phi') \cong E\Lambda\phi''$$

was used. The boundary conditions for the differential Eqs. (20b)–(20d) are

$$u_0 = v_0 = \phi_0 = u'_{L/2} = v'_{L/2} = \phi'_{L/2} = 0\,, \tag{21}$$

where $L/2$ refers to the column center.

Method of Numerical Analysis

Modification of Equilibrium Equations

Eqs. (20b)–(20d) can be rewritten as

$$E I_x (v'' - v_0'') + E I_{xy} (u'' - u_0'') + P v - P (x_0 - \bar{e}_x) \phi = E (\Gamma_{x0} - \Gamma_x) - P v_I, \quad (22a)$$

$$E I_y (u'' - u_0'') + E I_{xy} (v'' - v_0'') + P u + P (y_0 - \bar{e}_y) \phi = E (\Gamma_{y0} - \Gamma_y) - P u_I, \quad (22b)$$

$$P (x_0 - \bar{e}_x) (v'' - v_0'') - P (y_0 - \bar{e}_y) (u'' - u_0'') + (G K_T + \bar{K}_R + \bar{K}_I - P r_s^2) (\phi'' - \phi_0'') = E \{\Lambda \phi'' - (\Lambda \phi'')_0\} - P (x_0 - \bar{e}_x) (v_I'' - v_{I0}'') + P (y_0 - \bar{e}_y) u_I'' - u_{I0}''). \quad (22c)$$

These equations are identically satisfied at the column ends. Introducing new notations, $\bar{R}_x$ and $\bar{R}_y$, defined by

$$R_x = \frac{\bar{R}_x}{1 - \bar{R}_x} \frac{E I_x}{L} \quad (23a)$$

and

$$R_y = \frac{\bar{R}_y}{1 - \bar{R}_y} \frac{E I_y}{L} \quad (23b)$$

and considering Eqs. (13) and (14), the equilibrium Eqs. (20b)–(20d) at the column ends become

$$(1 - \bar{R}_x) E I_x v_0'' + (1 - \bar{R}_x) E I_{xy} u_0'' - \bar{R}_x \frac{E I_x}{L} \left(v_0' - \frac{b_2}{2} \phi_0'\right) = (1 - \bar{R}_x) P e_y - (1 - \bar{R}_x) E \Gamma_{x0}, \quad (24a)$$

$$(1 - \bar{R}_y) E I_y u_0'' + (1 - \bar{R}_y) E I_{xy} v_0'' - \bar{R}_y \frac{E I_y}{L} u_0' = (1 - \bar{R}_y) P e_x - (1 - \bar{R}_y) E \Gamma_{y0}, \quad (24b)$$

$$P (x_0 - \bar{e}_x) v_0'' - P (y_0 - \bar{e}_y) u_0'' + (G K_T + \bar{K}_R + \bar{K}_I - P r_s^2) \phi_0'' = E (\Lambda \phi'')_0 - P (x_0 - \bar{e}_x) v_{I0}'' + P (y_0 - \bar{e}_y) u_{I0}'', \quad (24c)$$

where L denotes the length of the column. These equations give additional boundary conditions for solving Eqs. (22). For numerical analysis it is convenient to express Eqs. (22) and (24) in non-dimensional form. This may be done by using the notations

$$\{U, V, U_I, V_I, X_0, Y_0, \bar{E}_x, \bar{E}_y, E_x, E_y\} = \frac{1}{r_0} \{u, v, u_I, v_I, x_0, y_0, \bar{e}_x, \bar{e}_y, e_x, e_y\}, \quad (25a)$$

$$Z = \frac{z}{L}, \quad P_x = \frac{\pi^2 E I_x}{L^2}, \quad P_y = \frac{\pi^2 E I_y}{L^2}, \quad P_z = \frac{G K_T + \bar{K}_R + \bar{K}_I}{r_0^2}, \quad \bar{P} = \frac{P}{P_x}. \quad (25b)$$

The resulting equations are shown in Appendix I.

Determination of Cross-Sectional Properties

In order to determine a number of cross-sectional properties defined in the foregoing sections, an angle section was divided into many small elements of area as shown in Fig. 8; the outstanding leg including the corner area is equally

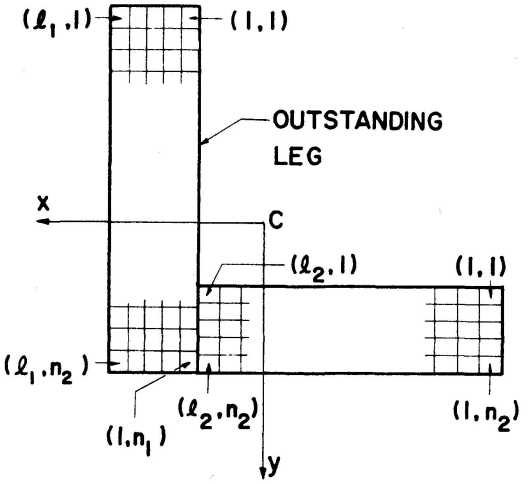

Fig. 8. Column Cross Section Showing Grid Networks.

divided into a total of l_1 columns and n_1 rows and the connected leg l_2 columns and n_2 rows. When determining the cross-sectional properties, it is assumed that the strains and coordinates of an element are represented by those at its centroid.

Finite Integral Representation

The differential Eqs. (34) under the boundary conditions (35) are solved numerically by the finite integral method [1]. The finite integral method is a numerical technique similar to the finite difference method except that numerical integrations are utilized instead of numerical differentiations. Let the half-length of the column be divided into m equal intervals and let the pivotal points i be named 0, 1, ..., m from the column end. In the present analysis, the quantities V_i'', U_i'' and ϕ_i'' at each pivotal point i are selected as unknown quantities, which makes a total of $3(m+1)$ unknowns. By integrating V_i'' to obtain V_i' and V_i, and by determining the integration constants from Eqs. (35a), one can obtain

$$V_i' = \int_0^{iH} V_i''\,dZ - \int_0^{1/2} V_i''\,dZ, \qquad V_i = \int_0^{iH}\int_0^{iH} V_i''\,dZ\,dZ - iH\int_0^{1/2} V_i''\,dZ\,dZ, \tag{26}$$

in which H denotes the non-dimensional interval length, which is equal to $1/2m$. Identical relations as Eqs. (26) are obtained for U_i'', U_i' and U_i and for ϕ_i'', ϕ_i' and ϕ_i. BROWN and TRAHAIR [1] have given the following numerical integration formulas:

$$\{F'\} = \frac{H}{12}[N]\{F''\} \qquad \text{for } F_i' = \int_0^{iH} F_i'' \, dZ, \qquad (i = 0, \ldots, m), \tag{27}$$

$$\{F\} = \frac{H^2}{144}[N][N]\{F''\} \quad \text{for } F_i = \int_0^{iH}\int_0^{iH} F_i'' \, dZ \, dZ, \qquad (i = 0, \ldots, m), \tag{28}$$

where $\{F''\}$, $\{F'\}$ and $\{F\}$ are, respectively, vectors of which components are F_i'', F_i' and F_i and the matrix $[N]$ is a square matrix of size $(m+1)$ which is given in Appendix II. Applying these formulas to Eqs. (26), the relations between $\{V'\}$ and $\{V''\}$ and between $\{V\}$ and $\{V''\}$ are obtained, in which $\{V\}$, $\{V'\}$ and $\{V''\}$ are vectors of which components are, respectively, V_i, V_i' and V_i'' $(i=0, 1, \ldots m)$. By using these relations, the equilibrium Eqs. (34b)–(34d) and the corresponding boundary conditions (35b)–(35d) may be reduced to the following $3(m+1)$ simultaneously equations with respect to V_i'', U_i'' and ϕ_i'' $(i=0, 1, \ldots m)$:

$$[A]\{\chi\} + \bar{P}[B]\{\chi\} = \{D\} + \bar{P}\{E\}, \tag{29}$$

where $\{\chi\}$ is a vector whose components are $3(m+1)$ unknown quantities V_i'', U_i'' and ϕ_i'' $(i=0, \ldots, m)$ and $[A]$ and $[B]$ are square matrices of size $3(m+1)$. The quantities related to the inelastic effects of the column, such as Γ_x, Γ_y and Λ, are assembled in the vector $\{D\}$. The vector $\{E\}$ represents the quantities with end moments due to eccentrical loading and with initial deflections.

Computational Procedure

The set of simultaneous equations (29) cannot be solved directly because the vector $\{D\}$ is an unknown function of $\{\chi\}$. Furthermore the equivalent eccentricities $\bar{e}_x$ and $\bar{e}_y$ in Eqs. (22) or $\bar{E}_x$ and $\bar{E}_y$ in Eqs. (34) are functions of end slope and the stiffness, R_x or $\bar{R}_x$, of the rotational spring may vary due to the yielding of the spring, and so the matrices $[A]$, $[B]$ and $\{E\}$ are also unknown functions of $\{\chi\}$. However, to avoid a time consuming trial and correction procedure involved in determining the matrices, the equivalent eccentricities and the rotational stiffness are assumed to be constant during each increment of $\{\chi\}$ so that those matrices $[A]$, $[B]$ and $\{E\}$ are specified by the previously determined $\{\chi\}$. By assuming this, Eqs. (29) can be directly solved in the elastic range of the column except for the first step of loading, where the values of $\bar{e}_x$ and $\bar{e}_y$ are still unknown. In the computational procedure the values of e_x and e_y were temporarily substituted for the values of $\bar{e}_x$ and $\bar{e}_y$, respectively, during the first step of loading, and after the solution $\{\chi\}$ and consequently $\bar{e}_x$ and $\bar{e}_y$ were obtained from Eqs. (29) and (14) the computations was again performed at the same load with the previously determined value of $\bar{e}_x$ and $\bar{e}_y$. The computational procedure after the column has entered the inelastic range is outlined below. In the statements, quantities with the superscript * represent the corresponding converged quantities from the previous

calculation and quantities with the prefix δ represent the corresponding increments from the previously converged values. These notations are consistent with those previously used.

1. Determine matrices $[A^*]$, $[B^*]$, $\{D^*\}$ and $\{E^*\}$ from $\{\chi^*\}$.
2. Assume trial values of $\{\delta\chi\}$ and $\{\delta\epsilon_c\}$, and determine trial values of $\{\chi\}$ and $\{\epsilon_c\}$. The quantities $\{\delta\epsilon_c\}$ and $\{\epsilon_c\}$ are determined at each pivotal point, and so they are, respectively, vectors of size $(m+1)$.
3. Determine $\{\delta D\}$ and consequently $\{D\}$ from $\{D\}=\{D^*\}+\{\delta D\}$.
4. Determine $\{\bar{P}\}=\left\{\frac{P}{P_x}\right\}$ from Eq. (34a) and average the values $\bar{P}$ to obtain $\bar{P}_c$. The quantity $\bar{P}$ is determined at each pivotal point, and so $\{\bar{P}\}$ is a vector of size $(m+1)$. The quantity $\bar{P}_c$ is used as a control value for non-dimensional axial thrust.
5. Determine the corrections of the assumed values of $\{\delta\chi\}$ and $\{\delta\epsilon_c\}$ from Eqs. (29) and (34a) by the Newton-Raphson method [10].
6. Check if the corrections of $\{\delta\chi\}$ and $\{\delta\epsilon_c\}$ satisfy the following rule of convergence:

$$\left|\frac{\delta(\delta q)}{q}\right| \leqq \mu,$$

where q denotes a value from $\{\chi\}$ and $\{\epsilon_c\}$, $\delta(\delta q)$ denotes the corresponding correction determined in computational step 5, and μ represents the tolerance tatio of convergence. The value of μ in this analysis is 0.003 for the convergence tests of $\{V''\}$ and $\{\epsilon_c\}$, and is 0.005 for those of $\{U''\}$ and $\{\phi''\}$. If above rule is not satisfied, add the corrections to the corresponding trial values of $\{\delta\chi\}$ and $\{\delta\epsilon_c\}$ to obtain the corrected values of $\{\delta\chi\}$ and $\{\delta\epsilon_c\}$ and repeat the procedure 2 through 6 with the corrected values of $\{\delta\chi\}$ and $\{\delta\epsilon_c\}$ as the new trial values.
7. Repeat steps 1 through 6 until the desired displacement is obtained.

Numerical Studies

In the subsequent articles, the results of numerical analysis for single-angle test columns, the details of which are reported elsewhere [6], [8], [10], are described. The tests were performed on equal and unequal leg steel angle columns (2 in. × 2 in. × 1/4 in. and 3 in. × 2 in. × 1/4 in. angles) whose ends were welded to web plates of structural Tee stubs (ST 61 I 7.5 of 8 in. long) to provide end restrains, such as shown in Fig. 1. The columns were loaded eccentrically through the webs of the Tee stubs with three different end bearing conditions (a), (b) and (c). In end condition (a), the axial load was directly applied on the flange surfaces of the end Tee stubs, and in end conditions (b) and (c) knife edge ends were used with the loading lines placed on the middle plane of the webs of the end Tee stubs and on the y axis, respectively.

In applying the theoretical analysis to the single-angle test columns, it is necessary to evaluate the end restraint parameters $\bar{R}_x$ and $\bar{R}_y$. For the purpose, the idealized column end assemblies shown in Fig. 9 are utilized in the case of end condition (a). These assemblies are assumed to be cantilever beams with cross-sections as indicated on the far right sides of Fig. 9. It is also assumed

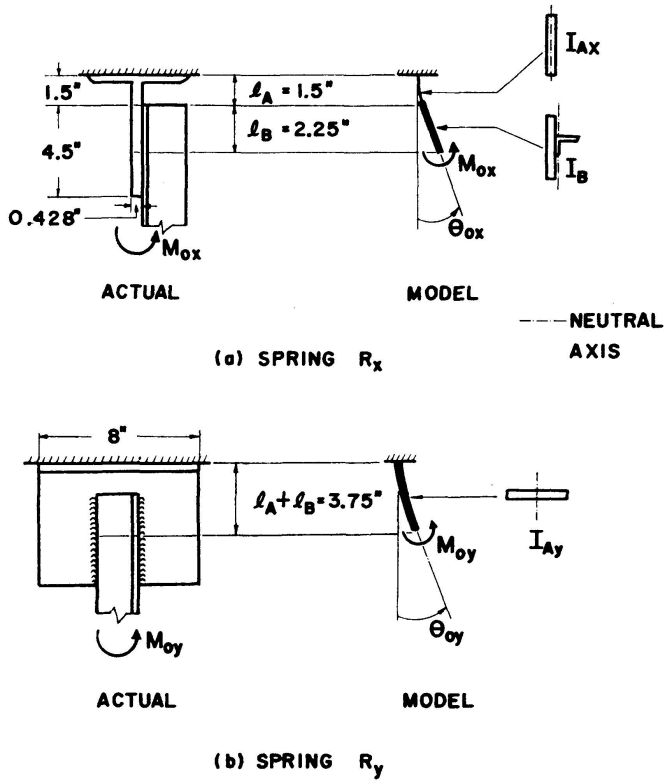

Fig. 9. Models for Determining the End Spring Stiffnesses.

that the moment-versus-rotation characteristics of these assemblies are uncoupled, and that the maximum value of the moment M_{0x} is equal to the fully plastic moment M_p, of the Tee stem alone about its weak principal axis. Thus the moment-versus-rotation characteristics of the assemblies can be determined as

$$\frac{M_{0x}}{\theta_{0x}} = \frac{1}{l_A/E\,I_{Ax}+l_B/E\,I_B}, \qquad \text{when } 0 \leqq \theta_{0x} \leqq \theta_p, \tag{30a}$$

$$\frac{M_{0x}}{\theta_{0x}} = \frac{1}{l_A/E\,I_{Ax}+l_B/E\,I_B}\,\frac{\theta_p}{\theta_{0x}}, \qquad \text{when } \theta_{0x} \geqq \theta_p \tag{30b}$$

and

$$\frac{M_{0y}}{\theta_{0y}} = \frac{E\,I_{Ay}}{l_A+l_B}, \tag{30c}$$

where the lengths l_A and l_B are defined in Fig. 9, I_{Ax} and I_{Ay} are, respectively, the moments of inertia of the Tee stem alone about the weak and strong principal axes, I_B is the moment of inertia of the Tee stem with the angle

about the centroidal axis shown in Fig. 9a, and θ_p is the end rotation of the assembly (a) at $M_{0x}=M_p$, namely

$$\theta_p = M_p\left(\frac{l_A}{E\,I_{Ax}}+\frac{l_B}{E\,I_B}\right). \tag{31}$$

From Eqs. (1), (23) and (30), the end restraint parameters $\bar{R}_x$ and $\bar{R}_y$ are given by

$$\bar{R}_x = \frac{1}{1+\left(\frac{l_A}{I_{Ax}}+\frac{l_B}{I_B}\right)\frac{I_x}{L}}, \qquad \text{when } 0\leqq\theta_{0x}\leqq\theta_p, \tag{32a}$$

$$\bar{R}_x = \frac{1}{1+\left(\frac{l_A}{I_{Ax}}+\frac{l_B}{I_B}\right)\frac{I_x}{L}\frac{\theta_{0x}}{\theta_p}}, \qquad \text{when } \theta_{0x}\geqq\theta_p \tag{32b}$$

and

$$\bar{R}_y = \frac{1}{1+\frac{l_A+l_B}{I_{Ay}}\frac{I_y}{L}}. \tag{32c}$$

The quantity θ_{0x} is equivalent to the absolute value of the end slope of the column at the location of the springs (see Fig. 3), that is

$$\theta_{0x} = \left|v_0'+v_{I0}'-\frac{b_2}{2}\phi_0'\right|.$$

In the case of end condition (b) the knife edges are placed parallel with the plane of the Tee stems so that the value of $\bar{R}_x$ is equal to zero and $\bar{R}_y$ is given by the same expression as Eq. (32c). In end condition (c) the knife edges are perpendicular to the plane of the Tee stems, and so the value of $\bar{R}_y$ is zero and $\bar{R}_x$ is given by the same expressions as Eqs. (32a) and (32b).

The computational procedure described previously was programmed in the FORTRAN IV language for an electronic digital computer. The IBM 360/50 computer located at the Sever Institute of Technology of Washington University was utilized for the numerical studies.

Comparison with Trahair's Elastic Solutions

Before the computer program was utilized for the elastic-plastic analysis of angle columns, sufficient runs were made to study elastic column behaviour and to compare the results with elastic solutions determined by TRAHAIR [8], [9]. Three problems shown in Table 1 are selected as the examples for the comparison. The angle columns for the three problems correspond to two of the test columns, and columns 2 and 3 in Table 1 show the corresponding test column numbers and end conditions. The cross-section of the angle is 2 in. × 2 in. × $^1/_4$ in. and the material is ASTM A 242 steel. The numbers of grids used for the cross-section were $l_1=3, n_1=24, l_2=21$ and $n_2=3$, and the number of divisions of the column length, m, was 6 throughout the problems. The values of the end restraint parameter $\bar{R}_x$ were determined from a simple model shown

Table 1. Data for Problems 101–103 (Elastic Analysis)

Problem Number	Test Column Properties[1] (Ref. 6)				End Restraint Parameters	
	Number	End Condition	Length, L, in inches	$\frac{L}{r_z}$	$\bar{R}_x$	$\bar{R}_y$
(1)	(2)	(3)	(4)	(5)	(6)	(7)
101	A-2-8	*b*	34.9	89.5	0	0.9999
102	A-2-8	*b*	34.9	89.5	0	1.0
103	A-1-8	*a*	33.9	86.8	0.757	0.9999

[1]) 2-in. × 2-in. × 1/4-in. angle of ASTM A 242 steel
$E = 29.4 \times 10^3$ ksi, $e_x = -0.41$ in., $e_y = 0.804$ in.

before, while the value of $\bar{R}_y$, 0.9999, is the value used by Trahair for an approximate fixed end condition along the x axis. In problem 102, the real fixed end condition $\bar{R}_y = 1$ was used for comparison. Neither initial deflections nor residual stresses were considered in the elastic problems.

The computed load versus mid-height deflection curves of problems 101 and 102 are presented in Fig. 10. The column dimensions in both problems are identical except for the assumed value of $\bar{R}_y$. When $\bar{R}_y$ is equal to 1.0, the equivalent eccentricity $\bar{e}_x$ defined by Eq. (14b) cannot be used because the value of R_y becomes infinite. In such case the value of $\bar{e}_x$ was automatically set to zero in the computer program because eccentricity of load does not make any sense in the direction of the fixed end and it is always equivalent to zero. Trahair's solutions given in reference [8] were converted into the deformations $u_{L/2}$, $v_{L/2}$ and $\phi_{L/2}$, and they are plotted in the same figure at

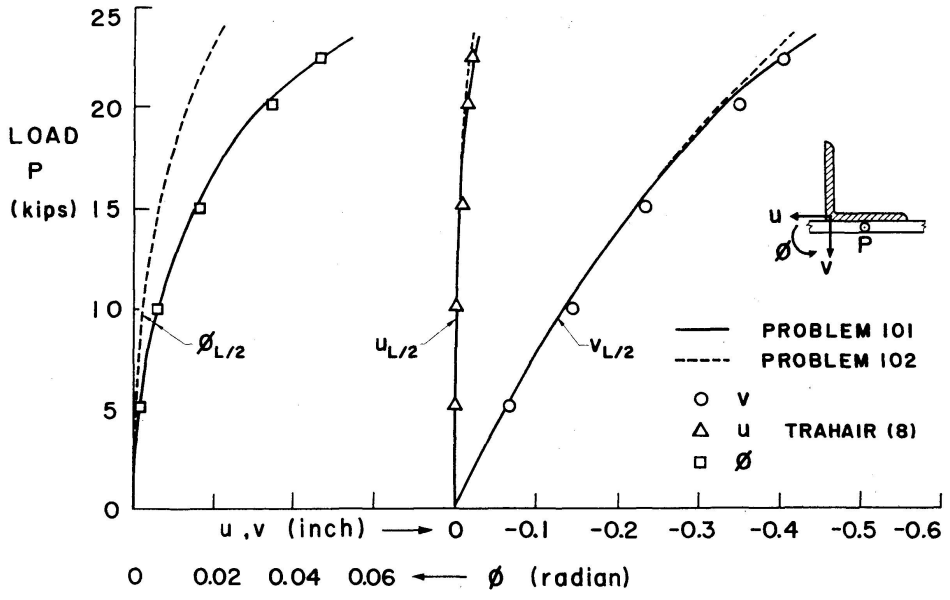

Fig. 10. Comparison of Elastic Solutions. Problems 101 and 102.

ordinates corresponding to 5, 10, 15, 20 and 22 kips. The agreement between the results of problem 101 and the Trahais's solutions is quite reasonable, whereas the results of problem 102 are very much different from the others in the torsional deformation $\phi_{L/2}$. The reason may be well explained when the difference of the equivalent eccentricity $\bar{e}_x$ between the two problems is evaluated. Fig. 12a shows the variations of the values of $\bar{e}_x$ and r_s^2 in problem 101. The quantity r_s^2 is defined in Eq. (18a), and it is a function of the equivalent eccentricities $\bar{e}_x$ and $\bar{e}_y$. The equivalent eccentricity $\bar{e}_y$ is, in this case, always equal to the real eccentricity e_y because the rotational stiffness R_y (or $\bar{R}_y$) is zero. The quantity $\bar{e}_x$ and r_s^2 are undetermined at loads less than 5 kips because the first loading step was 5 kips. Now, from Eq. (20d) with $\bar{K}_R = \bar{K}_I = \Lambda = v_I'' = u_I'' = 0$, the following relation may be obtained:

$$\phi = \frac{-P(x_0 - \bar{e}_x)v + P(y_0 - \bar{e}_y)u}{GK_T - Pr_s^2}, \tag{33}$$

because of the boundary conditions 21. This is one of the equilibrium equations which the solutions u, v and ϕ must satisfy. Since the deflection $u_{L/2}$ is very small compared with the deflection $v_{L/2}$ (see Fig. 10), the second term of the numerator of Eq. (33) may be neglected when the value of $\phi_{L/2}$ is evaluated. The magnitude of the denominator of Eq. (33) will not be very much different between problems 101 and 102 because the value of GK_T is very large compared with that of Pr_s^2 within the value of P under consideration. Thus the difference between the magnitudes of $\phi_{L/2}$ for the two problems will be dependent on the difference between the values of the first term of the numerator of Eq. (33) and, therefore, on the difference between the values of the quantity $(x_0 - \bar{e}_x)$ because the deflections $v_{L/2}$ are almost identical in both problems (see Fig. 10). The value of $\bar{e}_x$ is identically zero in problem 102, and so $x_0 - \bar{e}_x = x_0 = 0.46$ *in.* in problem 102. On the other hand, in problem 101, the value of $\bar{e}_x$ varies with P as shown in Fig. 12a. Take $P = 15$ kips, for instance, the value of $\bar{e}_x/e_x$ is about 1.4 and the value of e_x is -0.41 in., and so $x_0 - \bar{e}_x = 0.46 - 1.4x(-0.41)$ $= 1.03$ *in.* in problem 101. Therefore the value of $\phi_{L/2}$ in problem 101 will be $1.03/0.46 = 2.5$ times greater than that in problem 102 at load $P = 15$ kips. The conclusion quite agrees with the results shown in Fig. 10. Thus it has been confirmed that the difference of the results of $\phi_{L/2}$ between the two problems is mainly due to the difference of the values of $\bar{e}_x$. In a real column it would be impossible to realize a perfectly fixed end condition (i.e., $\bar{R}_x = 1$), and so the results of problem 101 will be more realistic than those of problem 102.

The computed load versus mid-height deflection curves for problem 103 are compared with Trahair's solutions in Fig. 11, and the corresponding load versus $\bar{e}_x$, $\bar{e}_y$ and r_s^2 curves are presented in Fig. 12b. As the axial thrust P becomes large, the deformations $v_{L/2}$ and $\phi_{L/2}$ determined by Trahair become slightly different from those obtained in the present numerical analysis. This may be due to the difference of the assumed value of $\bar{R}_x$, the numerical value

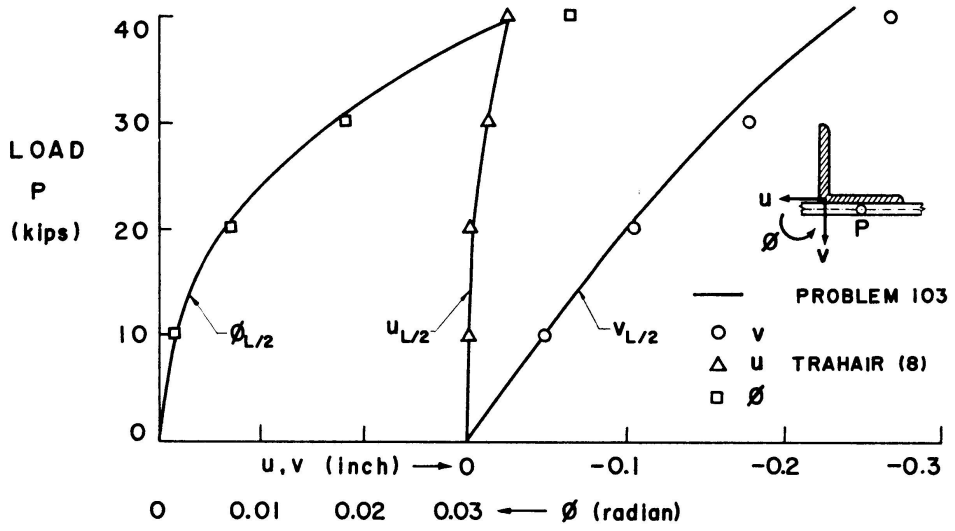

Fig. 11. Comparison of Elastic Solutions. Problem 103.

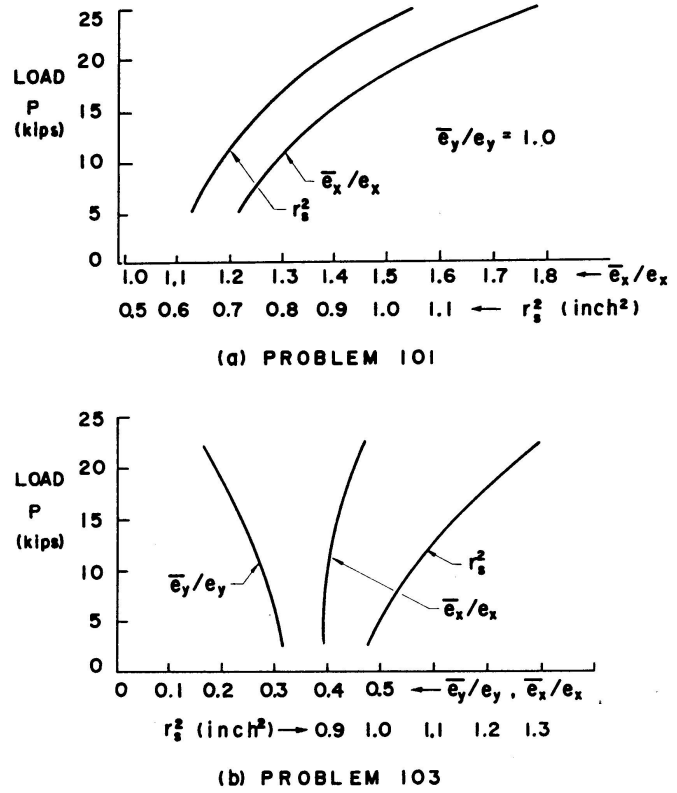

Fig. 12. Load Versus $\bar{e}_x$, $\bar{e}_y$ and r_s^2 Curves.

of which is not given in Trahair's paper. The ratio $\bar{e}_x/e_x$ is, in this case, less than 1.0 as shown in Fig. 12b and so the equivalent eccentricity $\bar{e}_x$ is smaller in magnitude than the real eccentricity.

Effects of Residual Stresses and Initial Deflections

Two columns were selected to examine the effects of residual stresses and initial deflections on the elastic-plastic behaviour of the columns. Those columns are equivalent to test columns A-2-8 and A-1-8, which were, respectively, tested under end conditions (b) and (a). Seven problems shown in Table 2 were run to analyze those columns under various combinations of presence of residual stresses and initial deflections. Problems 201 through 204 are for test column A-2-8, and Problems 205 through 207 for test column A-1-8. The values of $\bar{R}_x$ and $\bar{R}_y$ for each column were determined as mentioned before. The number of divisions of the column length, m, was 6, and the

Table 2. Effects of Residual Stresses and Initial Deflections

Problem Number	Residual Stress	Initial Deflection	Computed First Yielding Load, in kips		Maximum Load, P_{MAX}, in kips		Test Column Properties[1] (Ref. 6)
			Angle	Spring	Computed	Test	
(1)	(2)	(3)	(4)	(5)	(6)	(7)	(8)
201	None	None	16.0	—	18.2	16.9	Column Numb.: A-2-8 $L=34.9''$, $L/r_z=89.5$, $\bar{R}_x=0$, $\bar{R}_y=0.998$[2]
202	Yes	None	12.8	—	17.4		
203	None	Yes	13.6	—	16.2		
204	Yes	Yes	11.0	—	15.4		
205	None	None	27.0	24.7	28.91	29.0	Column Numb.: A-1-8 $L=33.9''$, $L/r_z=86.8$, $\bar{R}_x=0.757$, $\bar{R}_y=0.998$[2]
206	Yes	None	22.0	23.0	28.89		
207	Yes	Yes	23.0	23.0	27.90		

[1]) 2-in. × 2-in. × 1/4-in. angle of ASTM A 242 steel, $E = 29.4 \times 10^3$ ksi, $\sigma_Y = 50.9$ ksi, $e_x = -0.41$ in., $e_y = 0.804$ in.
[2]) Elastic Value.

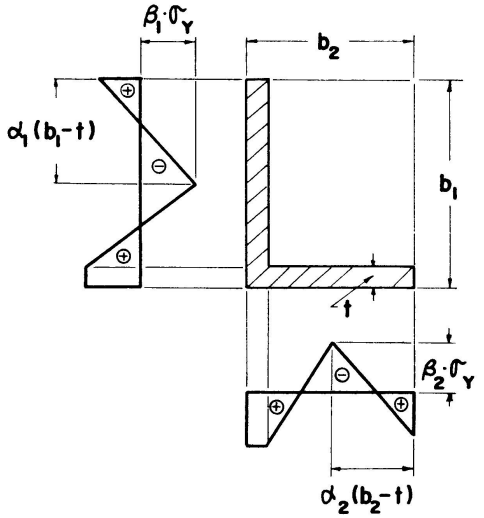

Fig. 13. Assumed Residual Stress Pattern.

numbers of grids for the cross-section were same as for the previous elastic analysis. The residual stress pattern of an angle cross-section was assumed to be as shown in Fig. 13. The four non-dimensional parameters α_1, α_2, β_1 and β_2 are sufficient to specify the whole pattern owing to the self-equilibrating conditions of residual stresses given by Eqs. (2). Since residual stresses were not measured, the assumed pattern was taken from the literature [7]. The values of α_1, α_2, β_1 and β_2 used in the present numerical studies are, respectively, 0.575, 0.575, -0.3 and -0.3. As for the initial deflections of the columns, it is assumed that the angle column has an initial deflection only in the direction of the outstanding leg before testing and that the deflected shape is expressed by a parabolic curve with a maximum center deflection, δ_0, equal to the standard mill tolerance for camber given in ASTM Specification A 6, that is

$$\delta_0 = \frac{L}{240},$$

where L denotes the length of the column in inches. When such an angle column is tested under end condition (a), the original deflected shape will change, an additional deflection is induced in the plane of the Tee stems and axial stresses due to bending will be produced in the angle because the bending axis of the original deflection is not a principal axis of the angle-section and because the flangles of the end Tees are fixed. Therefore the column will have initial stresses σ_I as well as initial deflections u_I and v_I. However, in the case of end conditions (b) and (c) tests, the additional deflections and stresses are all released at the start of testing because the knife edge ends were used in those tests. Consequently the initial deflected shape of the test column at the start of testing is the same as that before testing.

Fig. 14 shows the computed load versus mid-height deformations $v_{L/2}$ and

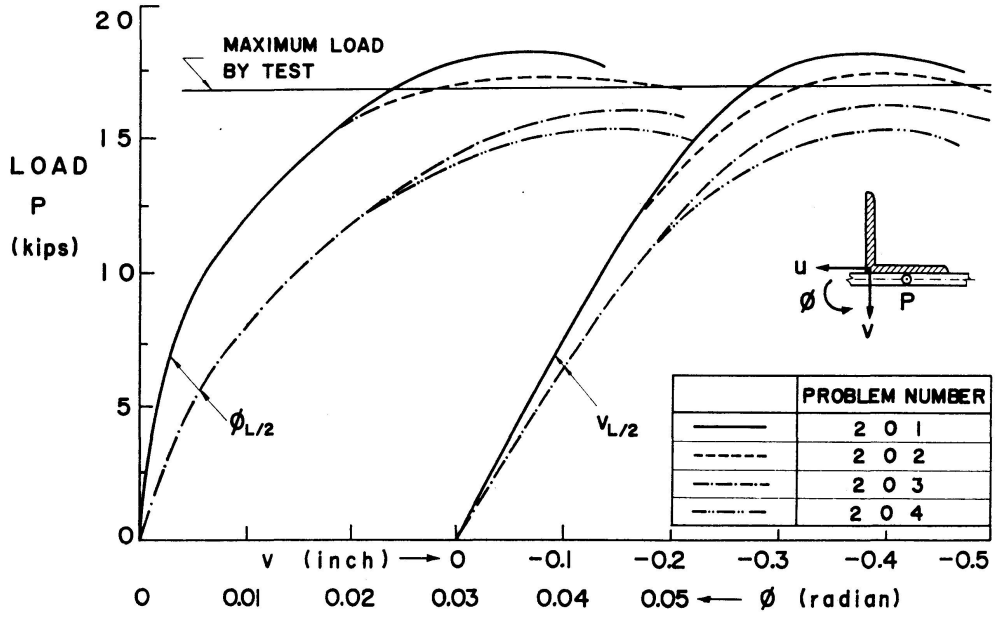

Fig. 14. Effects of Residual Stresses and Initial Deflections. Problems 201–204.

$\phi_{L/2}$ curves of problems 201 through 204, and Table 2 presents a summary of the computed first yielding loads and maximum loads together with the observed maximum load in the experiment of the A-2-8 column. The first yielding load of problem 202 is lower than that of problem 203, but the former has more inelastic reserve strength than the latter case. The effect of residual stresses on the maximum loads is relatively insignificant, and the presence of residual stresses (problems 202 and 204) reduces the maximum loads by 4 percent. On the other hand, the reduction of the maximum loads by initial deflections (problems 203 and 204) is about 10 percent, which is relatively significant. It is noteworthy that the presence of initial deflections considerably affects the torsional deformations. The experimental maximum load lies between the computed maximum load of problem 202, where only the effect of residual stresses is considered, and of problem 203, where only the effect of initial deflections is taken into account. This seems to be quite reasonable because the severest situation was assumed for the initial deflections.

The load versus mid-height deflection curves of problems 205 through 207 are presented in Fig. 15, and the computed first yielding and maximum loads are summarized in Table 2 together with the experimental maximum load of column A-1-8. The computed first yielding loads are shown for both column and the end spring about the x-axis. Since an elastic-perfectly plastic moment-versus-rotation curve was assumed for the end spring, the first yielding load of the end spring implies the load at which a plastic hinge forms in the spring. Those first yielding loads of the end spring were always below the corresponding computed maximum loads. The effects of residual stresses and initial deflections are both quite insignificant. The strength of this type of column seems to be greatly influenced by the yield stress level of the end spring instead of the residual stresses and initial deflections. The experimental maximum load

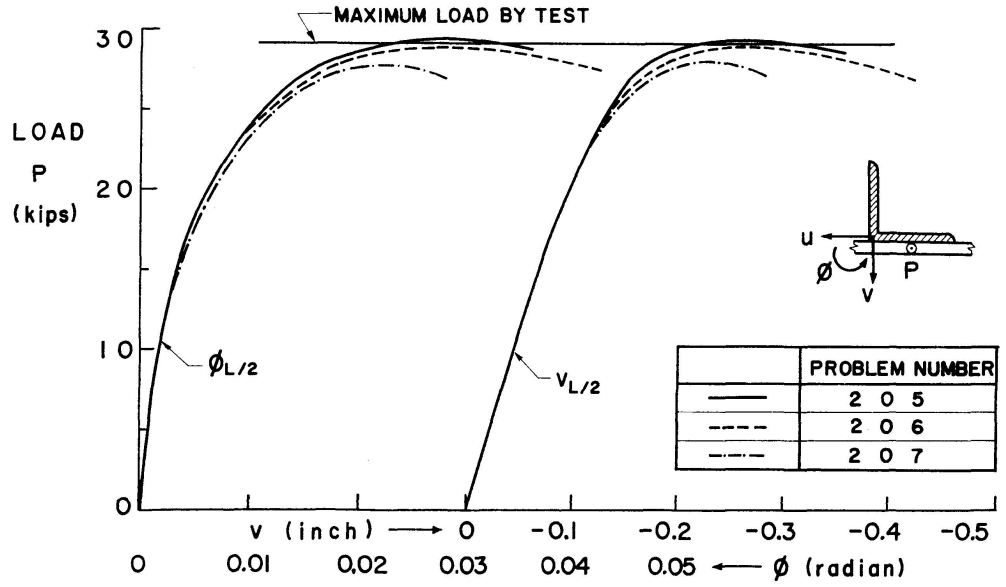

Fig. 15. Effects of Residual Stresses and Initial Deflections. Problems 205–207.

is almost equal to the predicted maximum loads of problems 205 and 206 and is slightly higher than the prediction of problem 207.

It will be concluded from the above discussion that the presence of the assumed initial deflections has a relatively marked effect on the maximum strength of the column under end condition (b). However, since initial deflections were not measured in the test program, their effect will not be considered in the subsequent numerical studies and only the effect of residual stresses will be taken into consideration.

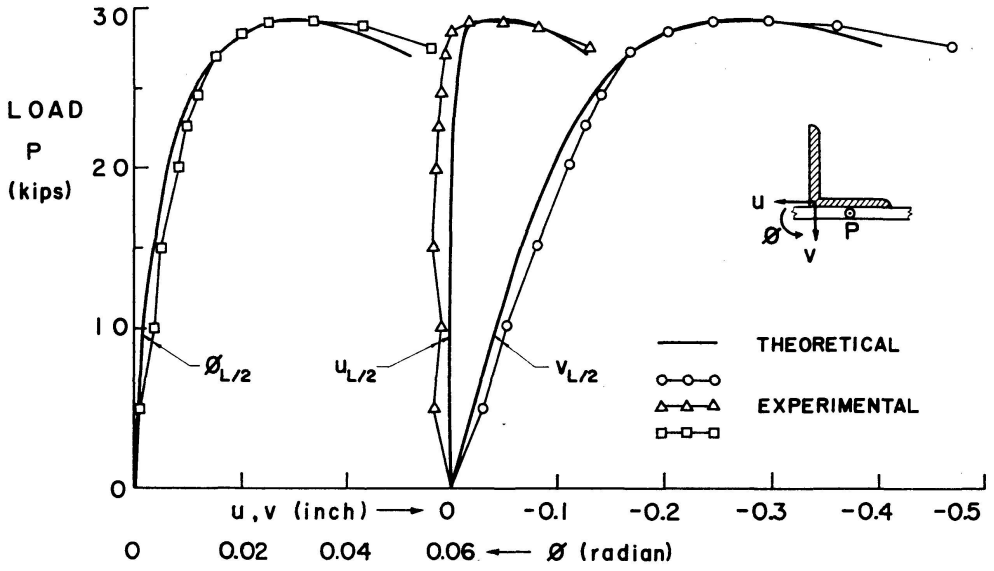

Fig. 16. Experimental and Theoretical Load-Deflection Curves. Column A-1-8.

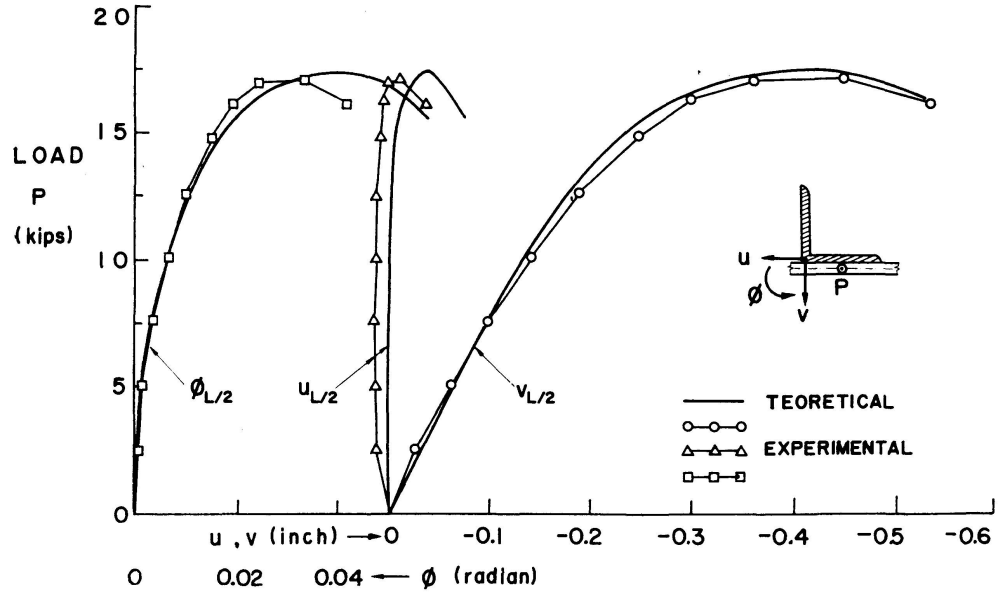

Fig. 17. Experimental and Theoretical Load-Deflection Curves. Column A-2-8.

Table 3. Comparison of Theory and Test

Problem Number	Test Column Properties (Ref. 6)									P_{MAX}/P_Y		Column 12 / Column 11	Remarks	
	Number	End Condition	$\bar{R}_x$ [1]	$\bar{R}_y$	L, in inches	$\frac{L}{r_z}$	λ_x	e_x, in inches	e_y, in inches	Test	Computed			
(1)	(2)	(3)	(4)	(5)	(6)	(7)	(8)	(9)	(10)	(11)	(12)	(13)	(14)	
301	A-1-1	*a*	0.879	0.999	79.1	202	1.72	–0.41	0.804	0.318	0.356	0.894		
302	A-1-2	*a*	0.851	0.999	62.0	159	1.37	–0.41	0.804	0.485	0.459	1.056		
303	A-1-5	*a*	0.809	0.999	46.0	118	1.01	–0.41	0.804	0.531	0.570	0.933	$2'' \times 2'' \times 1/4''$ Angle	
304	A-1-8	*a*	0.757	0.998	33.9	86.8	0.745	–0.41	0.804	0.617	0.605	1.020	$E = 29.4 \times 10^3$ ksi	
305	A-1-11	*a*	0.661	0.997	21.8	56.3	0.477	–0.41	0.804	0.669	0.673	0.994	$G = 11.3 \times 10^3$ ksi	
306	A-2-1	*b*	0.0	0.999	80.1	205	1.74	–0.41	0.804	0.151	0.150	1.007	$\sigma_Y = 50.9$ ksi	
307	A-2-3	*b*	0.0	0.999	55.0	141	1.20	–0.41	0.804	0.241	0.241	1.000		
308	A-2-8	*b*	0.0	0.998	34.9	89.5	0.761	–0.41	0.804	0.356	0.367	0.970		
309	A-2-11	*b*	0.0	0.997	23.0	59.0	0.500	–0.41	0.804	0.472	0.450	1.048		
310	A-3-8	*c*	0.763	0.0	35.0	89.8	0.770	0.0	0.804	0.454	0.496	0.915		
311	C-1-1	*a*	0.629	0.999	54.9	128	0.795	–0.51	1.20	0.461	0.454	1.015	LLO [2]	$3'' \times 2'' \times 1/4''$ Angle
312	C-1-3	*a*	0.533	0.998	37.0	87.7	0.537	–0.51	1.20	0.546	0.530	1.030		$E = 29.3 \times 10^3$ ksi
313	C-3-1	*b*	0.0	0.999	56.0	133	0.811	–0.51	1.20	0.361	0.352	1.025		$G = 11.3 \times 10^3$ ksi
314	C-3-3	*b*	0.0	0.998	37.8	89.8	0.548	–0.51	1.20	0.457	0.437	1.045		$\sigma_Y = 57.5$ ksi
315	C-2-1	*a*	0.819	0.996	55.0	131	1.41	–0.51	0.704	0.366	0.381	0.960	SLO [3]	
316	C-2-3	*a*	0.732	0.994	36.9	87.5	0.942	–0.51	0.704	0.522	0.519	1.005		
317	C-4-1	*b*	0.0	0.996	56.2	133	1.44	–0.51	0.704	0.184	0.184	1.0		
318	C-4-3	*b*	0.0	0.994	38.0	89.8	0.967	–0.51	0.704	0.279	0.270	1.034		

[1]) Elastic Value. [2]) LLO: Long Leg Outstanding. [3]) SLO: Short Leg Outstanding.

Comparison with Test Results

A total of 18 problems listed in Table 3 were analyzed to make comparison with the test results. The number of divisions of the column length and the numbers of grids used for partitioning the cross-section were both the same as those in the previous elastic-plastic problems except for the unequal leg angle columns with the long leg outstanding (marked LLO in Table 3), where n_1 was increased to 36. The computed load versus midheight deformation curves for column numbers A-1-8 and A-2-8 are, respectively, compared with the corresponding test results in Figs. 16 and 17. The computed results are generally in adequate agreement with the test results, especially in view of the fact that the end conditions and the load eccentricities of the test columns are somewhat uncertain and that initial deflections and initial twists of the test columns are neglected in the theoretical calculations. The computed maximum loads P_{MAX} of 18 columns are tabulated in Table 3, together with the non-dimensional values of P_{MAX}, P_{MAX}/P_Y, where P_Y is the squash load of the angle section. The calculated and measured values of maximum loads differ by a maximum of 10.6 percent (column A-1-1) and the mean value of the ratios is 0.997.

In order to compare the predictions with the test results of other columns than the 18 columns shown above, the maximum strength curves were determined from the calculated maximum loads. Figs. 18 and 19 illustrate those maximum strength curves against the non-dimensional slenderness ratio λ_x for end conditions (a) and (b), respectively. There are three theoretical curve for the equal-leg angle of A 242 steel and the other two curves represent the theoretical curves for the unequal leg angle with the long leg out and with the short leg out, respectively. The non-dimensional slenderness ratio

$$\lambda_x = \frac{L}{r_x}\frac{1}{\pi}\sqrt{\frac{\sigma_Y}{E}}$$

was used to represent the slenderness because the test columns with end conditions (a) and (b) tended to deflect mainly in the directions of the outstanding leg. Using the slenderness ratio λ_x is convenient for plotting test results of columns with different material properties. All the experimental maximum loads for end conditions (a) and (b) are, respectively plotted in Figs. 18 and 19. Fig. 19 also contains the plots of Foehl's test results [4]. He tested seven single-angle columns of various cross-sections under an end condition very similar to end condition (b). He also used structural Tee stubs (ST 6 I 15.9 of ASTM A 36 steel) at the column ends, and axial load was applied through steel cylinders, which were welded to the outside face of the flange of the structural Tees in the direction of the Tee stems, to the test column ends. Since the stem thickness of the Tee stubs is slightly different from that in the present tests (i.e., 0.350 in. whereas 0.428 in. in the tests of this paper), the value of eccen-

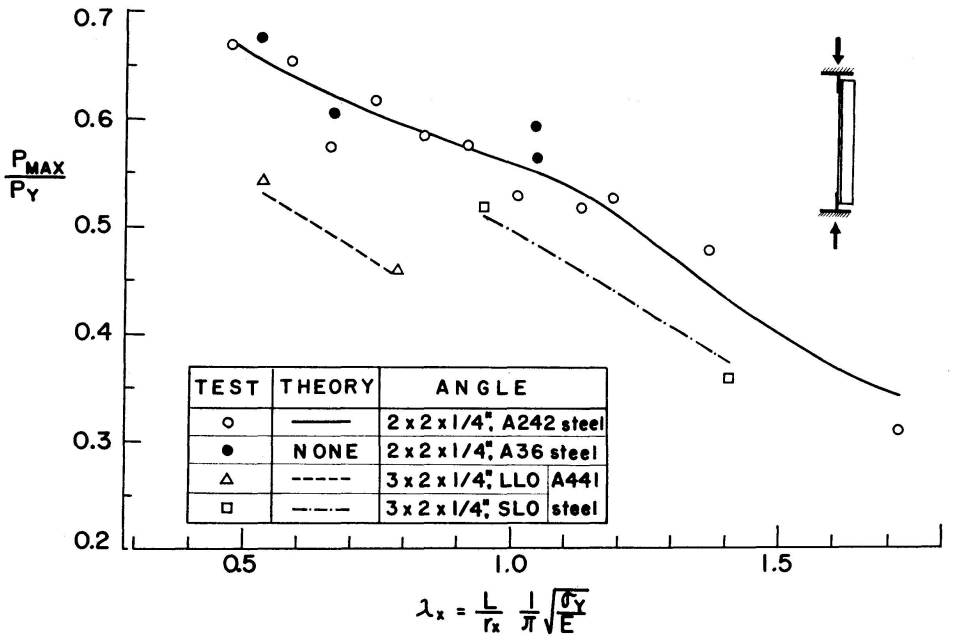

Fig. 18. Comparison of Theoretical and Experimental Maximum Loads, End Condition (a).

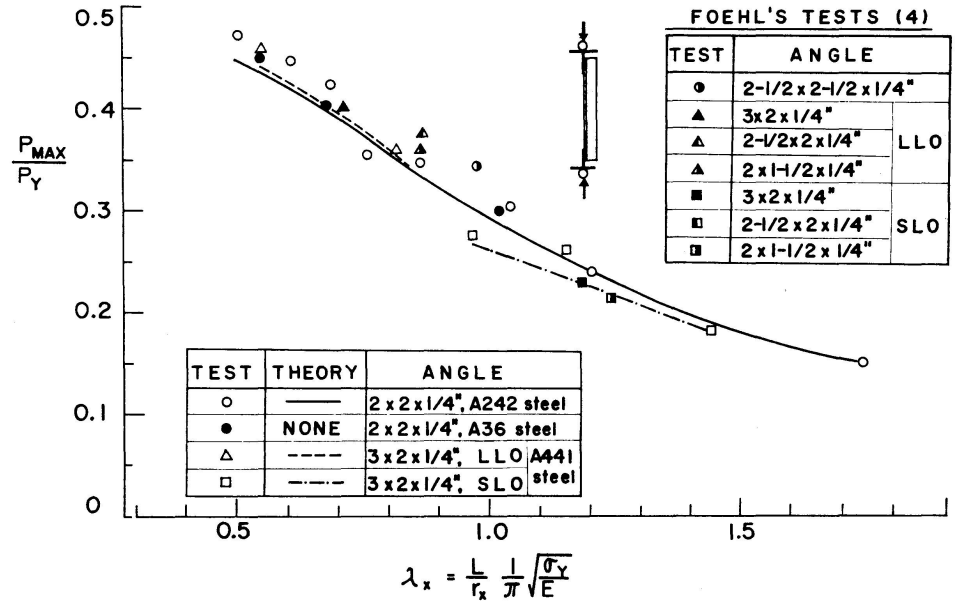

Fig. 19. Comparison of Theoretical and Experimental Maximum Loads, End Condition (b).

tricity e_y is also slightly different even if the cross-sectional dimensions are same. No adjustment was, however, made when Foehl's test results were plotted in Fig. 19. Although some scatter of the test results is observed especially in end condition (a), the correlation between theory and test is reasonably good in both end conditions. Foehl's test results of 3 in. × 2 in. × 1/4 in. angle columns (marked ▲ for LLO and ■ for SLO in Fig. 19) excellently agree with the corresponding maximum strength curves. In end condition (a) the maximum strength curves have marked difference depending on the shape and the

attitude of angle, while in end condition (b) the difference becomes very small and the maximum strength curve for 2 in. × 2 in. × 1/4 in. angle of A 242 steel may be used for the predictions of the other shapes of angle with reasonable accuracy.

Conclusions

A numerical procedure has been presented for determining the elastic-plastic behaviour of single-angle columns. These single-angle columns are treated as non-sway end-restrained columns loaded eccentircally. The end restraints are represented by two rotational springs, one is an elastic-perfectly spring and the other is an elastic spring, at both column ends. The effects of residual stresses and initial deflections are allowed for in the procedure. Numerical results in the elastic range are compared with results based on the solution of TRAHAIR [8]. The results from the proposed numerical procedure are generally in good agreement with Trahair's results. Two selected single-angle columns equivalent to test columns with end conditions (a) and (b) reported in [6], [8], [10] were solved to examine the effects of residual stresses, initial deflections and their combination on the elastic-plastic behaviour of those columns. It was found that the effects of residual stresses are quite insignificant in both columns, but that the presence of the assumed initial deflection, which is considered to be the severest situation for the columns, has a relatively marked effect on the maximum strength of the column with end condition (b). A total of 18 single-angle columns were solved to make comparisons with the test results described in reference [6], [8], [10]. The computed load-versus-deformation curves are generally in adequate agreement with the test results. The computed and measured values of the column strengths differ by a maximum of 10.6 percent, and the average value of the ratios of the computed column strengths to the measured column strengths is 0.996. Maximum strength curves plotted against the non-dimensional slenderness ratio λ_x, were developed for end conditions (a) and (b) columns in order to make further comparisons with other test results. It is demonstrated that the predictions from the maximum strength curves compare well with the experimental maximum loads of the columns having a wide-range of slenderness ratios.

Acknowledgement

This paper forms a part of research projects on biaxial behavior of steel members sponsered by the Steel Joist Institute and the National Science Foundation (Grant GK 10604). It was performed in the Structural Division of the Civil and Environmental Engineering Department of Washington

University in St. Louis. The help of Washington University Computing Facilities through the National Science Foundation Grant G-22296 is also acknowledged.

Keywords

Angle, *beam-columns*, bending, *deformation*, *inelastic analysis*, stability, structural engineering, torsion.

Appendix I. Nondimensional Form of the Equilibrium Equations and Boundary Conditions

Equilibrium Equations

$$\bar{P} = \frac{EA}{P_x}\left(\epsilon_c + \frac{\Gamma}{A}\right), \tag{34a}$$

$$v'' - v_0'' + \frac{I_{xy}}{I_x}(U'' - U_0'') + \pi^2 \bar{P} V - \pi^2 \bar{P}(X_0 - \bar{E}_x)\phi = \frac{L^2}{r_0 I_x}(\Gamma_{x0} - \Gamma_x) - \pi^2 \bar{P} V_I, \tag{34b}$$

$$(U'' - U_0'') + \frac{I_{xy}}{I_y}(V'' - V_0'') + \pi^2 \frac{P_x}{P_y}\bar{P} U + \pi^2 \frac{P_x}{P_y}\bar{P}(Y_0 - \bar{E}_y)\phi = \frac{L^2}{r_0 I_y}(\Gamma_{y0} - \Gamma_y) - \pi^2 \frac{P_x}{P_y}\bar{P} U_I, \tag{34c}$$

$$\bar{P}(X_0 - \bar{E}_x)(V'' - V_0'') - \bar{P}(Y_0 - \bar{E}_y)(U'' - U_0'') + \left(\frac{P_z}{P_x} - \bar{P}\frac{r_s^2}{r_0^2}\right)(\phi'' - \phi_0'') = \frac{E}{r_0^2 P_x}\{A\phi'' - (A\phi'')_0\} - \bar{P}(X_0 - \bar{E}_x)(V_I'' - V_{I0}'') + \bar{P}(Y_0 - \bar{E}_y)(U_I'' - U_{I0}''). \tag{34d}$$

Boundary Conditions

$$U_0 = V_0 = \phi_0 = U_{1/2}' = V_{1/2}' = \phi_{1/2}' = 0, \tag{35a}$$

$$(1 - \bar{R}_x) V_0'' + (1 - \bar{R}_x)\frac{I_{xy}}{I_x} U_0'' - \bar{R}_x\left(V_0' - \frac{b_2}{2 r_0}\phi_0'\right) = -\frac{L^2}{r_0 I_x}(1 - \bar{R}_x)\Gamma_{x0} + \pi^2 (1 - \bar{R}_x)\bar{P} E_y, \tag{35b}$$

$$(1 - \bar{R}_y) U_0'' + (1 - \bar{R}_y)\frac{I_{xy}}{I_y} V_0'' - \bar{R}_y U_0' = -\frac{L^2}{r_0 I_y}(1 - \bar{R}_y)\Gamma_{y0} + \pi^2\left(\frac{P_x}{P_y}\right)(1 - \bar{R}_y)\bar{P} E_x, \tag{35c}$$

$$\bar{P}(X_0-\bar{E}_x)V_0''-\bar{P}(Y_0-\bar{E}_y)U_0''+\left(\frac{P_z}{P_x}-\bar{P}\frac{r_s^2}{r_0^2}\right)\phi_0''= \frac{E}{r_0^2 P_x}(A\phi'')_0-\bar{P}(X_0-\bar{E}_x)V_{I0}''+\bar{P}(Y_0-\bar{E}_y)U_{I0}''. \tag{35d}$$

It should be noted that primes in these equations are differentiation with respect to Z instead of z.

Appendix II. Matrix [N]

The expression for matrix $[N]$ is shown for $m=6$, that is for 6 divisions of half of the column length.

$$[N]=\begin{bmatrix} 0 & 0 & 0 & 0 & 0 & 0 & 0 \\ 5 & 8 & -1 & 0 & 0 & 0 & 0 \\ 4 & 16 & 4 & 0 & 0 & 0 & 0 \\ 4 & 16 & 9 & 8 & -1 & 0 & 0 \\ 4 & 16 & 8 & 16 & 4 & 0 & 0 \\ 4 & 16 & 8 & 16 & 9 & 8 & -1 \\ 4 & 16 & 8 & 16 & 8 & 16 & 4 \end{bmatrix}.$$

Appendix III. Notation

The following symbols are used in this paper.

A	Area of cross-section.
$[A]$	A matrix.
$[B]$	A matrix.
C	Centroid of a cross-section.
$\{D\}$	A vector.
E	Modulus of elasticity.
$\{E\}$	A vector.
E_x, E_y	Nondimensional eccentricity of load in the x and y direction.
$\bar{E}_x, \bar{E}_y$	Nondimensional equivalent eccentricity of load in the x and y direction.
e_x, e_y	Eccentricity of load in the x and y direction.
$\bar{e}_x, \bar{e}_y$	Equivalent eccentricity in the x and y direction.
F	Function of Z.
G	Shear modulus.
H	Nondimensional interval length.
I_{Ax}, I_{Ay}, I_B	Moments of inertia defined in Fig. 9.
I_x, I_y	Moment of inertia about the x and y axis.
I_{xy}	Product of inertia with respect to the x and y axes.

K_T	St. Venant's torsion constant.
$\bar{K}, \bar{K}_R, \bar{K}_I$	Cross-sectional constants defined by Eqs. (17), (18e) and (18f), respectively.
L	Effective column length.
l_1, l_2	Number of partitions of cross-section defined in Fig. 8.
l_A, l_B	Length defined in Fig. 9.
M_{Ix}, M_{Iy}	Initial moment about the x and y axis.
M_{0x}, M_{0y}	End moment about the x and y axis.
$\bar{M}_{0x}, \bar{M}_{0y}$	End moment about the x and y axis due to loading.
M_p	Fully plastic moment of the web of end Tee stub.
M_x, M_y, M_z	Moment about the x, y and z axis.
$M_\xi^{(e)}, M_\eta^{(e)}, M_\zeta^{(e)}$	External moment about the ξ, η and ζ axis.
m	Number of intervals.
$[N]$	Square matrices.
n_1, n_2	Number of partitions of cross-section defined in Fig. 8.
P	Axial load.
P_{MAX}	Experimental maximum load, maximum strength of a column.
P_x, P_y, P_z	Constants defined by Eq. (25b).
P_Y	Axial load corresponding to yield stress level.
$\bar{P}$	P/P_x.
$\{\bar{P}\}$	A vector of which component represents $\bar{P}$ at each pivotal point.
$\bar{P}_c$	Average value of components of $\{\bar{P}\}$.
$P_\zeta^{(e)}$	External axial force in the ζ direction.
p	Superscript specifying plastic strain component.
q	Component of vector.
R_x, R_y	Rotational stiffness of end spring about the x and y axis.
$\bar{R}_x, \bar{R}_y$	End restraint parameters defined by Eqs. (23).
r_0, r_s	Cross-sectional constants defined by Eqs. (18b) and (18a).
r_x, r_z	Radius of gyration of angle section about the x and weak principal axis.
S	Shear center.
sgn	Signum function.
t	Thickness of an angle leg.
U	Nondimensional deflection of the shear center in the x direction.
U_I	Nondimensional initial deflection of the shear center in the x direction.
U_i	Deflection U at pivotal point i.
u	Deflection of the shear center in the x direction.
u_I	Initial deflection of the shear center in the x direction.
V	Nondimensional deflection of the shear center in te y direction.
V_I	Nondimensional initial deflection of the shear center in the y direction.
V_i	Deflection V at pivotal point i.

v	Deflection of the shear center in the y direction.
v_I	Initial deflection of the shear center in the y direction.
X_0	Nondimensional coordinate of the shear center.
x	Coordinate of any point on a cross-section.
x_0	Coordinate of the shear center.
x'	Coordinate of a point in an initially deformed position.
Y_0	Nondimensional coordinate of the shear center.
y	Coordinate of any point on a cross-section.
y_0	Coordinate of the shear center.
y'	Coordinate of a point in an initially deformed position.
Z	Nondimensional centroidal longitudinal axis.
z	Centroidal longitudinal axis.
α_1, α_2	Residual stress parameters defined in Fig. 13.
β_1, β_2	Residual stress parameters defined in Fig. 13.
β_x, β_y	Cross-sectional constants defined by Eqs. (18c) and (18d), respectively.
$\Gamma, \Gamma_x, \Gamma_y$	Cross-sectional constants defined by Eqs. (11).
δ	Prefix specifying increment.
δ_0	Maximum initial deflection.
ϵ, ϵ^*	Normal strain in the z direction.
ϵ_c, ϵ_c^*	Compressive normal strain on the centroid.
ϵ_Y	Yield strain.
$\{\epsilon_c\}$	A vector of which component represents ϵ_c at each pivotal point.
ζ	Centroidal longitudinal axis of a deformed member.
η	Coordinate of a point in a deformed cross-section.
θ_{0x}, θ_{0y}	End slope of a column about the x and y axis.
θ_p	End rotation of end Tee web corresponding to M_p.
Λ	Cross-sectional constant defined by Eq. (18g).
λ_x	Nondimensional slenderness ratio about the x axis.
μ	Tolerance ratio in convergence tests.
ξ	Coordinate of a point in a deformed cross-section.
$\sum$	Summation.
σ, σ^*	Normal stress in the z direction.
σ_I	Initial stress.
σ_R	Residual stress.
σ_Y	Static yield stress level.
Φ_x, Φ_x^*	Curvature in the z-x plane.
Φ_y, Φ_y^*	Curvature in the z-y plane.
ϕ	Angle of twist.
ϕ_i	Angle of twist at a pivotal point i.
$\{\chi\}$	A vector.

Appendix IV. References

1. Brown, P. T., and Trahair, N. S.: Finite Integral Solution of Differential Equations. Research Report No. R 85, School of Civil Engineering, The University of Sydney, Sept. 1967.
2. Chen, W. F., and Santathadaporn, S.: Review of Column Behaviour Under Biaxial Loading. ASCE, Vol. 94, No. ST 12, Journal of the Structural Division, Proc. Paper 6316, Dec. 1968.
3. Culver, C. G.: Initial Imperfections in Biaxial Bending. ASCE, Vol. 92, No. ST 3, Proc. Paper 4846, Journal of the Structural Division, June, 1966.
4. Foehl, P. J.: Direct Method of Designing Single Angle Struts in Welded Trusses. In Design Book for Welding, Lincoln Electric Company, Nov. 1948.
5. Galambos, T. V.: Structural Members and Frames. Prentice-Hall, Inc., Englewood Cliffs, N. J. 1968.
6. Galambos, T. V., Usami, T., and Trahair, N. S.: Eccentrically Loaded Single Angle Columns. Research Report No. 11, Structural Division, Civil and Environmental Engineering Dept., Washington University, St. Louis, Mo., Aug. 1969.
7. Kato, B., ed.: Residual Stresses and Buckling (in Japanese). Journal of the Japan Society of Steel Construction, Vol. 3, No. 16, 1967.
8. Trahair, N. S., Usami, T., and Galambos, T. V.: Eccentrically Loaded Single Angle Columns. Research Report No. 11, Washington University, Department of Civil and Environmental Engineering, Aug. 1969.
9. Trahair, N. S.: Restrained Elastic Beam-Columns. ASCE, Vol. 95, No. ST 12, Journal of the Structural Division, Proc. Paper 6941, Dec. 1969.
10. Usami, T.: Restrained Single-Angle Columns under Biaxial Bending. Dissertation presented to Washington University, at St. Louis, Mo., in 1971, in partial fulfillment of the requirements for the degree of Doctor of Science.

Summary

A numerical procedure for determining the elastic-plastic behaviour of single-angle columns loaded eccentrically is presented. The analysis allows for the effects of biaxial bending, twisting and end restraints. Residual stresses and initial deflections of the columns are accounted for in the procedure. The numerical results are compared with test results of single angle columns, and good agreement is generally observed.

Résumé

On présente un procédé numérique pour la détermination du comportement élastique-plastique des colonnes en cornières chargées excentriquement. L'analyse comprend l'influence de la flexion biaxiale, les déformations torsionnelles et le serrage des extrémités des colonnes. Le procédé comprend également l'effet des tensions résiduelles et des courbures initiales. Les résultats numériques comparés avec les résultats expérimentaux ont démontré une bonne concordance.

Zusammenfassung

Es wird ein numerisches Verfahren für die Berechnung des elastisch-plastischen Bereiches und der Traglast von aussermittig belasteten Stahlstützen aus einzelnen Winkelprofilen vorgelegt. Die Berechnung berücksichtigt den Einfluss der zweiachsigen Biegung, die Torsionsverdrillung und die Einspannung der Stabenden sowie die Eigenspannungen und die Vorkrümmungen der Stabachse. Die Resultate der Berechnung werden mit Versuchsergebnissen verglichen, wobei eine allgemein gute Übereinstimmung von Theorie und Versuch beobachtet wurde.